Journal of Solid Mechanics Vol. 9, No. 4 (2017) pp. 878-890

Effect of Submerged Arc Welding Parameter on Crack Growth Energy on St37

J.A. Khodaii [1], A. Mostafapour [2, *], M.R. Khoshravan [2]

[1]*Department of Mechanical Engineering ,Amirkabir University of Technology, Tehran, Iran*
[2]*Department of Mechanical Engineering ,University of Tabriz, Tabriz, Iran*

Received 7 August 2017; accepted 11 October 2017

ABSTRACT

In this article the influence of welding parameters such as electrical current, feed rate and stick out on crack growth energy was investigated. Therefore, prepared specimens were welded in various conditions. Using the Minitab software, 18 states of 36 possible states were chosen and applied. Then a crack was crated on the weld metal and the force-displacement diagram was plotted. Comparison of results shows that in high electricity current, the extra heat flux is the dominant factor, which causes coarse grains of microstructures. On the other hand, in low electricity current, lack of fusion and penetration reduce the crack propagation energy. Furthermore, the neural network could predict the amount of energy with high accuracy.

Keywords : Submerged arc welding; Crack growth energy; Welding parameter; Optimization.

1 INTRODUCTION

SUBMERGED arc welding (SAW) is one of the most important technologies in huge structures' attachments like bridges, pressure vessels etc. during which electrical arc is hidden under specific powder of flux. The ability to perform automated and safe process because of undercover formation of arc and complete protection of weld pool are main reasons of the vast use of this technology. In contrary, one of the main disadvantages of this process is the high heat flux applied to the weld pool which makes appearance of defects in the weld pool more possible [1], [2], [3]. Generally, the quality of welded joint is dependent on the shape of weld metal. The weld shape is in turn a function of welding parameters such as feed rate, electrical current, preheat temperature etc. [2], [4]. It is also noteworthy that the SAW has a nonlinear behavior toward these parameters [5]. Artificial Intelligent (A.I) has been approached as a highly efficacious method in modeling of complex systems in recent years and many researchers have employed that in modeling of this process [6], [7]. A neural network has appropriate ability in learning and modeling of complex input and output parameters.

In recent years, some activities have been done in modeling the electrical current, feed rate and preheat temperature as input parameters; weld metal shape and strength as output parameters and eventually the quantity of output parameters have been estimated [8]. Juang et al [6] tried to optimize welding parameters by Taguchi method. Duga et al [9] have shown that more than 80% of structures' failure is due to fracture or crack propagation. Hasson et al. [10] investigated the fracture toughness of HY-130 steel weld and base metal. They have used the gas metal arc (GMA) weld and gas tungsten arc (GTA) weld. The HY-130 weld metal deposited by GMAW had lower crack initiation energy (JIC) value than the HY-130 steel base metal. It was attributed primarily to the higher oxygen

*Corresponding author. Tel.: +98 413 3354153; Fax: +98 413 3354153.
E-mail address: a-mostafapur@tabrizu.ac.ir (A.Mostafapur).

content of the weld metal. The HY-130, which was welded by GTAW, had a higher fracture toughness compared to the HY-130 base metal. Thus, lower heat input of GTA welding was shown to cause the highest fracture resistance. Hari Om et al [11] investigated the effect of wire feed rate on width of Heat Affected Zone (HAZ) in SAW. Their observations showed the direct relation of the wire feed rate and the HAZ width. In another word, the more the feed rate, the more the HAZ width. In addition, HAZ width linearly increases as heat input increases. Shen et al [12] investigated the effect of heat input in SAW. Their study revealed that bead reinforcement, bead width, penetration depth, HAZ size, deposition area and penetration area have direct relationship with heat input. Also electrode melting efficiency upon heat input has a maximum point. More accurately, it increases initially and falls after passing a maximum point. Cretegny and Saxena [13] performed high temperature fracture toughness tests on welded specimens of 1Cr- 1Mo-1-4V. They employed Gas Metal Arc (GMA) weld method. A wide range of fracture toughness values was obtained for weld metals, while for homogenous materials the value of JIC was typically unique. The yield strength mismatch between the base metal and the weld metal was found to directly influencing the fracture toughness behavior. Zuniga et al. [14] performed the fracture toughness test on samples of MMA in as-welded and stress-relieved conditions, and compared the results. They observed that the fracture toughness of the as-welded material is more reduced in comparison with the stress-relieved condition at a temperature of 200^{o}C. The fracture toughness of the MMA weld metal in the stress-relieved condition has a higher value at 200^{o}C than at 300^{o}C. On the other hand, the fracture toughness of the MMA weld metal in the as-welded condition is lower at 200^{o}C than at 300^{o}C. SAW has widespread applications in huge structural attachments like bridges and pressure vessels, and these structures are highly vulnerable to failure as a result of crack growth or fracture. As a result, investigation of fracture toughness in SAW and effect of process parameters on crack growth energy not only is beneficial, but also seems crucial.

This article aims to evaluate the effect of electrical current, feed rate and stick out in SAW on crack growth energy. To do so, initially a back propagating network (BPN) is used to model the welding process. This neural network has a multi-layer network handing network extra performance in nonlinear cases, which results in its wide application in parameter estimation. Furthermore, experiment design in Taguchi method is carried out. According to the experiment design, 21 specimens were prepared and were welded in various conditions. It is followed by measurement of crack propagation energy in specimens. Eventually an intelligent system was designed to estimate the join crack propagation energy based on input parameters.

2 THEORY

To analysis and determine material resistance on crack propagation, two methods exist:

- Stress concentration theory
- Energy release rate theory

In stress concentration theory, stress intensity factor (K) is defined. When this parameter gets its critical value, the crack propagates. On the other hand, the second theory expresses that crack propagation energy stores in the bulk and the crack grows when it reaches its critical value. General explanation about this theory comes next.

2.1 Energy release rate theory

The Griffith energy balance for fracture of brittle material, implicates that crack growth occurs when the required energy of crack longitude formation exists. For a unit thickness plane, the crack grows if:

$$\frac{d}{da}(U - F + W) = 0 \tag{1}$$

where U is the absorbed elastic energy, F is the external work done and W is the required energy to crack formation. Thus energy release rate and crack growth resistance is defined as:

$$\frac{d(F - U)}{da} = G \tag{2}$$

$$R = \frac{dw}{da} \tag{3}$$

As shown in Fig. 1, for a plane under load P that is displaced as dv, the value of external works:

$$G = \frac{d}{da}(F - U_l) = \frac{1}{B}(P\frac{dV}{da} - \frac{dU_l}{da}) \tag{4}$$

Also:

$$C = \frac{V}{P} \tag{5}$$

where C is the compliance. For plane without crack that whose length, width and thickness are L,W and B respectively, the compliance is:

$$C = \frac{L}{WBE} \tag{6}$$

which E is the Young's modulus. So the elastic energy of the plane with crack will be:

$$U_l = \frac{1}{2}PV = \frac{1}{2}CP^2 \tag{7}$$

Having Eqs.(5), (6) and (7) substituted in (4), the result will be:

$$G = \frac{1}{B}\left(\frac{\delta U_l}{\delta a}\right)P = \frac{1}{B}\left(\frac{\delta U_l}{\delta a}\right)V = \frac{P^2}{2B}\frac{\delta C}{\delta a} \tag{8}$$

So the required energy for crack propagating that is proportional with critical load in mode I is, equal to:

$$G_C = \frac{P_C^2}{2B}\frac{dc}{da} \tag{9}$$

The crack propagates when the energy release rate surpasses its critical value.

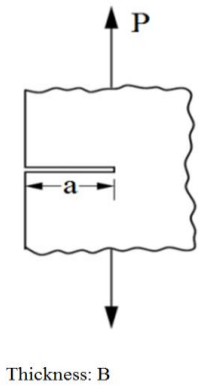

Fig.1
Plane with crack under Load [15].

3 EXPERIMENTAL DETAILS

3.1 Specimen definition

The specimen used in this experiment is a compact test' sample that was fabricated based on ASTM E 399-74. Geometry and dimensions of specimen according to standard is shown in Fig. 2. Also since most of fracture of structures occur in mode I, in this research the specimen was under load of this mode. The load was applied statically and jaws move with constant speed of $50\frac{mm}{\min}$. In this research structural steel (St 37) was investigated whose mechanical properties is shown in Table 1.

Table 1
Mechanical property of Structural steel.

Parameter	Value
Yield Strength (*MPa*)	215
Tensile Strength (*MPa*)	360
Yong modulus (*GPa*)	300

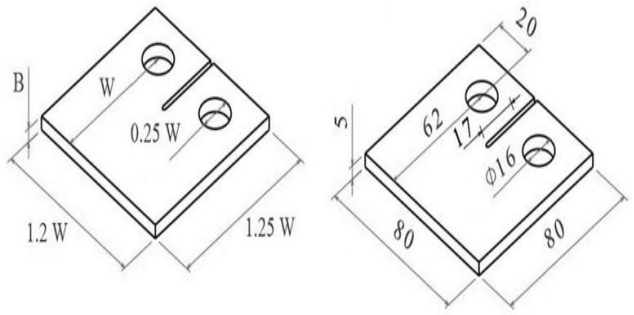

Fig.2
Standard Compact test specimen [15].

3.2 Equipment

In this investigation the Zwick Z100 Machine was used to plot the force-displacement diagram. Also the G1202 submerged arc welding machine was used to weld specimens. To create a perpendicular edge, the Baykal HNC 3100X25 shear machine was used.

3.3 Experimental description

Primarily, 42 specimens were cut from a 5*mm* thick plane. Specimen dimensions are shown in Fig. 3. In order to investigate the influence of various parameters on crack growth energy, the specimen was welded under several conditions and then numbered. The number and amount of each parameter at every level are given in Table 2. To optimize the experiment, using the Minitab software, 18 states of 36 possible states were selected and applied on samples.

Table 2
Parameters value at each layer

Parameter	I	II	III	IIII
Electrical current (A)	350	400	450	
Feed rate ($\frac{mm}{\min}$)	450	500	550	600
Stick Out (*mm*)	15	20	25	

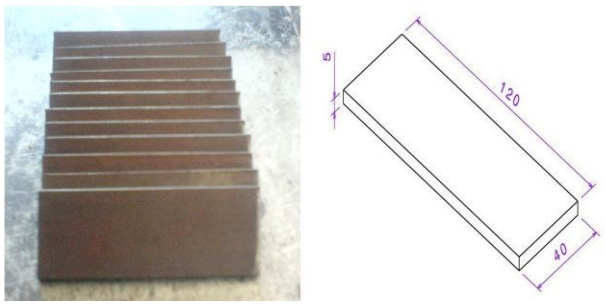

Fig.3
Primary specimen dimension.

The amount of parameter for each specimen is reported in Table 3. To avoid the arc blow, specimens were settled on 200X200X10 *mm* plane (Fig. 4). For formation of appropriate heat flux, the specimens were cooled naturally and when they reached room temperature, the slag was cut. Due to instability of the arc at both ends, the length of specimens was chosen a bit longer, and extra areas were cut subsequently as shown in Fig. 5. Then the specimens were ground in equal thickness (Fig. 6). Next, using the surface plate and height gauge, two points with coordination of (20, 18) and (60, 18) were specified. Later they were used to create 16*mm* holes. The line passing through holes' centers should be exactly perpendicular to the weld line in order to create a tensile stress only. It also prevents the growth of crack from weld to base metal (Fig.7).

Table 3
Parameter value for each specimen.

Number	Feed rate (*mm/Min*)	Current (A)	Stick Out (*mm*)
1	550	400	25
2	450	350	15
3	450	450	25
4	550	350	15
5	600	450	15
6	500	350	25
7	550	350	25
8	450	450	15
9	550	350	20
10	500	400	15
11	500	400	25
12	450	400	20
13	60	400	20
14	500	400	20
15	550	450	25
16	500	450	25
17	500	350	15
18	450	400	15
19	450	350	20
20	600	350	20
21	450	400	25

Fig.4
Welding specimens on plate to avoidance of arc blow.

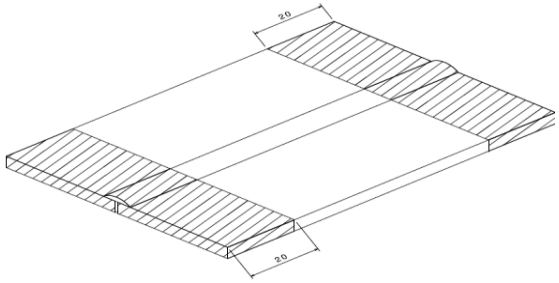

Fig.5
Trimming the instable part of specimen.

Fig.6
Specimen after grinding.

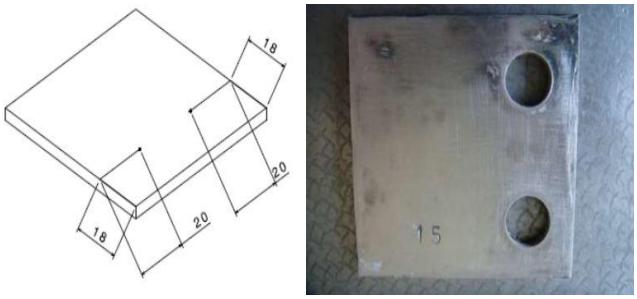

Fig.7
Marking and drilling of specimens.

In the next step, a 33*mm* long crack was formed on weld. To do so, firstly specimens were arranged on surface plate and marked as shown in Fig.8. Next the specimens clamped on machine to start the test. Fig. 9 shows the specimen during and after test. For each sample, after starting the test and passing the critical value, crack began to growth several millimeters. At this moment the test was stopped and jaws return to their primary position. The value of crack length was measured and recorded by Set Square and millimetric paper which was been glued on specimens. All steps were repeated four times. Force-displacement diagram for specimen 5 is shown in Fig.10. Then these diagrams were superposed to achieve the amount of maximum force in each step and the proportional displacement as shown in Fig.11. The amount of crack length, maximum force and the proportional displacement are given in Table 4. Using these data and Eq.(5) the amount of compliance for various crack length was calculated. In the next step, the compliance-crack lengths diagram was drawn. This diagram is a power curve and equation of this diagram was extracted using Excel software.

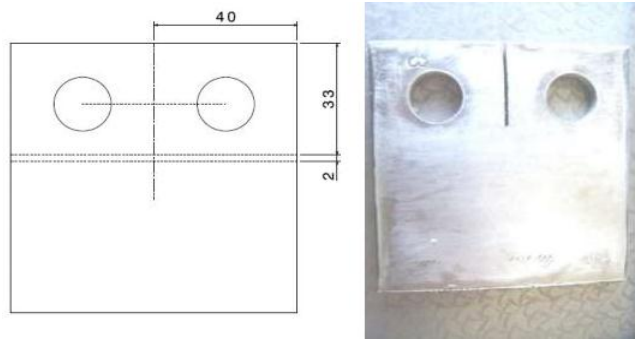

Fig.8
Marking and crack creating on specimens.

Fig.9
Specimens on test machine and after test.

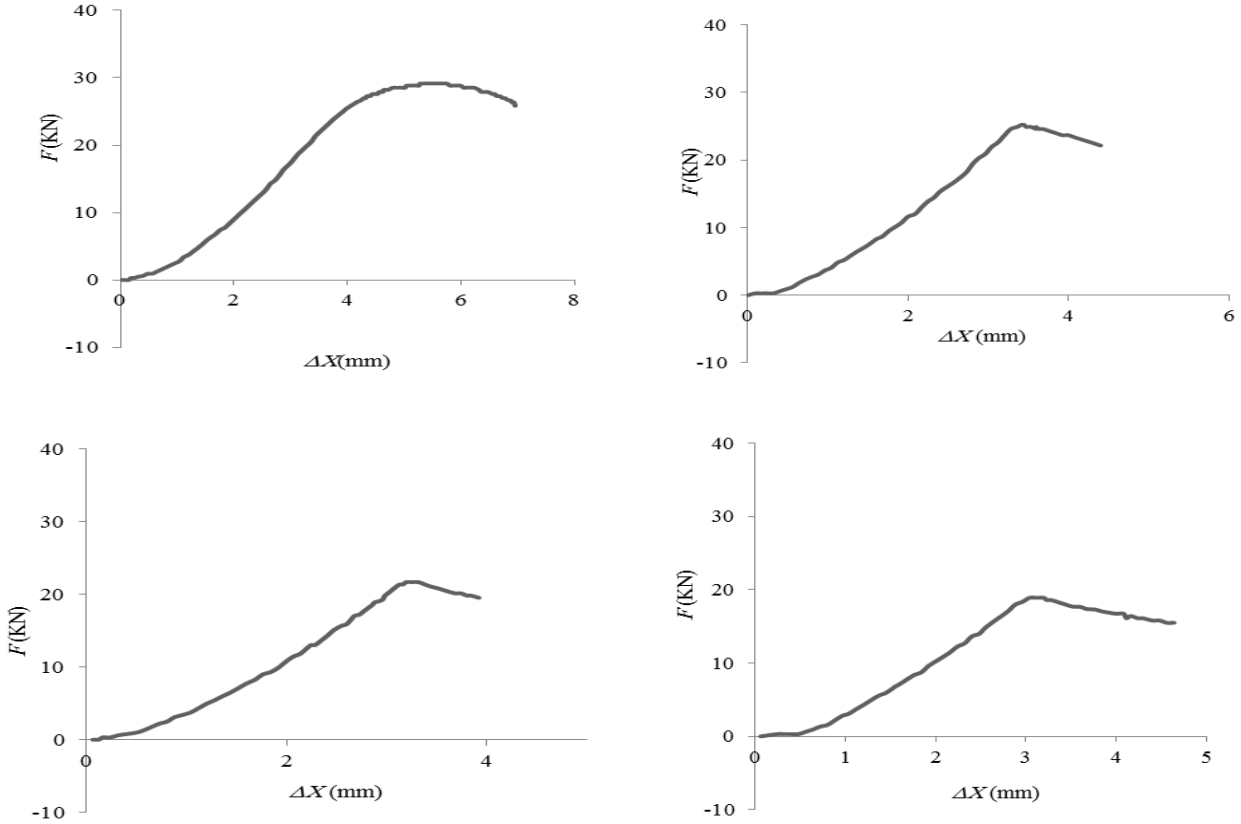

Fig.10
Force-Displacement Diagram for specimen 5.

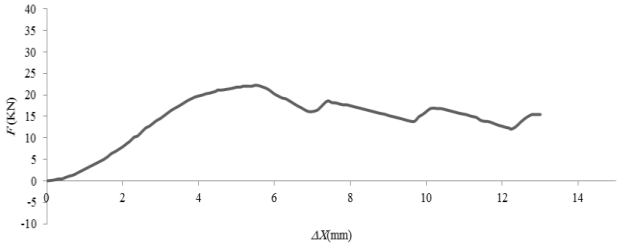

Fig.11
Extracting maximum force and its proportional displacement from superposed diagram.

Table 4
Crack length, maximum force and its proportional displacement.

Num	F_0 (*KN*)	F_1 (*KN*)	F_2 (*KN*)	F_3 (*KN*)	δ_0 (*mm*)	δ_1 (*mm*)	δ_2 (*mm*)	δ_3 (*mm*)	a_0 (*mm*)	a_1 (*mm*)	a_2 (*mm*)	a_3 (*mm*)
1	29	26.5	23.5	21.5	5.1	6.4	7.8	9.2	17	26	32	40
2	30	25	22	18.5	6.1	8.5	10	11.6	17	22	28	33
3	35	31.5	21	17.5	11.5	12.3	18.2	25	17	22	28	33
4	21	18	13.5	8	4.2	5.4	6.2	7.4	17	25	36	42
5	29	25	21.5	18.5	5.3	7.8	9.5	10.85	17	22	27	32
6	23.5	19.5	17	12	3.9	5.8	6.35	8.25	17	25	32	39
7	22	14.5	10.5	5.5	4.2	5.8	6.8	8.7	17	25	33	40
8	27.5	24	21.5	16.5	5.6	9.1	10.5	12.5	17	24	28	33
9	18	15	11.5	8.5	2.5	4.6	5.4	6.3	17	27	32	38
10	33	29.5	21.5	17.5	3.9	5.8	6.95	8.3	17	22	30	35
11	28	24.5	22.5	18.5	5.6	9.6	10.95	12.95	17	22	27	33
12	24.5	21.5	15.5	10.5	4.3	5.6	6.2	7.1	17	25	30	38
13	35	23.5	20.5	16.5	5.7	7.4	8.3	9.5	17	30	36	42
14	28	25	22.5	18.5	4.6	6.6	8	9.25	17	22	27	32
15	31.5	27.5	21.5	20	6.2	9.2	12.5	13.7	17	22	30	35
16	31	24	12.5	7.5	5.15	6.0	6.9	7.7	17	22	30	37
17	21	14	11	6	3.7	5.1	5.9	6.6	17	25	33	45
18	29	25	23	21	6.4	8.2	10.9	12.4	17	22	27	32

These equations were further derived and the derivative equation for each specimen was obtained. Compliance-crack length diagram, it's equation and derivative equation for specimen 10 are shown in Fig.12. Then, the amount of compliance derivate for various crack lengths was obtained using the compliance derivate equation. Next, using the Eq.(9) and the amount of compliance derivative; the mount of crack propagating energy was calculated. The compliance derivative and crack growth energy for various crack lengths are given in Table 5. Eventually to obtain the amount of independent of thickness crack growth energy (G_{Ic}) for each specimen, crack growth energy-crack length diagram was drawn. The diagram for specimen 11 is shown in Fig.13. Also the amount of crack growth energy of the 17*mm*-long crack and one's of thickness-independent crack growth energy are given in Table 6.

Table 5
Compliance derivative and crack propagating energy for various crack length.

Num	C'_0 (*1/N*)	C'_1 (*1/N*)	C'_2 (*1/N*)	C'_3 (*1/N*)	G_0 (*N/mm*)	G_1 (*N/mm*)	G_2 (*N/mm*)	G_3 (*N/mm*)
1	0.016	0.033	0.048	0.072	2.03	2.31	2.65	2.82
2	0.027	0.042	0.064	0.085	2.43	2.62	3.09	3.19
3	0.022	0.036	0.057	0.078	2.39	2.57	2.92	3.01
4	0.016	0.032	0.061	0.080	0.71	1.04	1.12	1.18
5	0.022	0.035	0.052	0.072	1.85	2.19	2.40	2.46
6	0.015	0.030	0.047	0.066	0.83	1.14	1.36	1.46
7	0.019	0.040	0.070	0.103	0.62	0.84	1.07	1.17
8	0.015	0.029	0.038	0.050	1.13	1.67	1.76	1.80
9	0.017	0.039	0.054	0.074	0.69	1.11	1.19	1.20
10	0.017	0.027	0.049	0.080	1.85	2.25	2.39	2.42
11	0.017	0.027	0.038	0.055	1.33	1.62	1.89	1.92
12	0.015	0.03	0.042	0.064	0.90	1.39	1.51	1.60
13	0.015	0.044	0.066	0.082	1.84	2.43	2.77	2.85
14	0.017	0.026	0.038	0.052	1.33	1.63	1.92	2.00
15	0.021	0.034	0.061	0.082	2.08	2.57	2.82	2.90
16	0.022	0.036	0.064	0.096	2.01	2.37	2.49	2.54
17	0.021	0.043	0.072	0.129	0.92	1.27	1.40	1.44
18	0.018	0.029	0.042	0.057	1.51	1.81	2.22	2.41

Table 6
Crack propagating energy for 17*mm* crack and Independent of thickness crack propagating energy.

Num	G_c (*N/mm*)	G_{Ic} (*N/mm*)
1	2.03	2.80
2	2.02	2.90
3	2.39	3.01
4	0.71	1.25
5	1.85	2.46
6	0.83	1.41
7	0.62	1.17
8	1.13	1.80
9	0.69	1.20
10	1.85	2.42
11	1.33	1.92
12	0.9	1.6
13	1.84	2.85
14	1.33	1.97
15	2.08	2.88
16	2.01	2.54
17	0.92	1.44
18	1.51	2.34

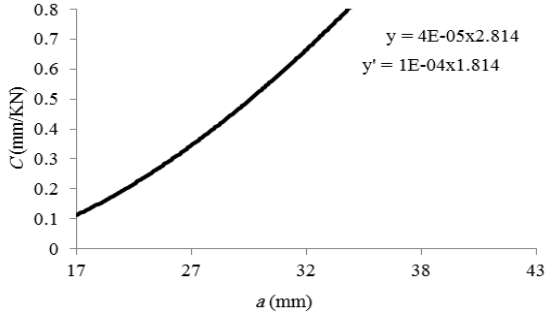

Fig.12
Crack propagating energy-crack length diagram for specimen 11.

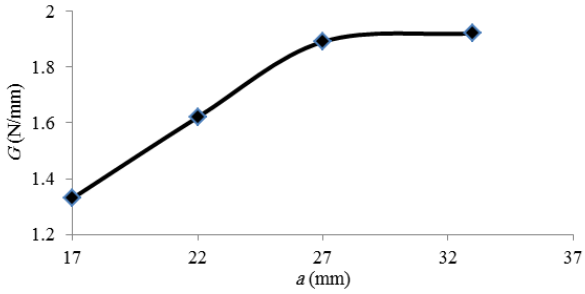

Fig.13
Compliance-crack length diagram, its equation and derivative equation for specimen 10.

Using the experimental data, a neural intelligent system was designed. To do so using the Matlab software, a three layered back propagating network was designed, an input layer, output layer and hidden layer. The input layer has three inputs including electrical current, feed rate and stick out. The output layer has 1 output namely independent of thickness crack growth energy (G_{Ic}). The number of hidden layers was chosen by try and error in order to achieve the desired precision. Finally, the value of 14 for layers was chosen. The Sigmund binary function used as transformation function is:

$$f(x) = \frac{2}{1+\exp(-x)} - 1 \tag{10}$$

The result of each test is composed of training data that contains the value of input and output parameters. The neurons relation in network is determined by weighted values. The amount of these weighted vectors was chosen randomly in first step. Network estimates the amount of output parameter using input parameter at each step. If there was an error between real and estimated values, the error was propagated to former step and weighted values were amended until reaching a network error less than 0.000001. The network training errors diagram and training proceeding to achieve desired accuracy after 1064 step is shown in Figs. 14 and 15.

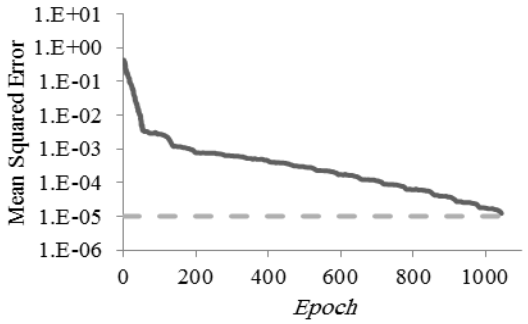

Fig.14
Networks training error diagram to obtain desired precision.

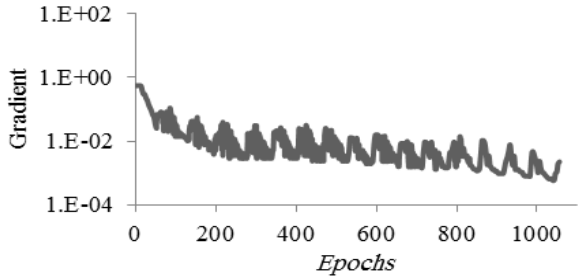

(a)

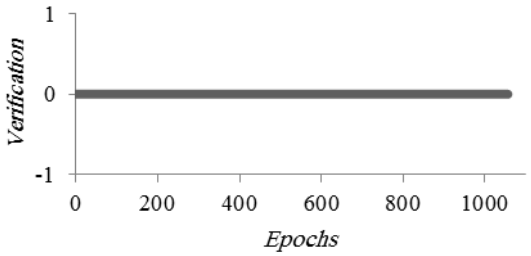

(b)

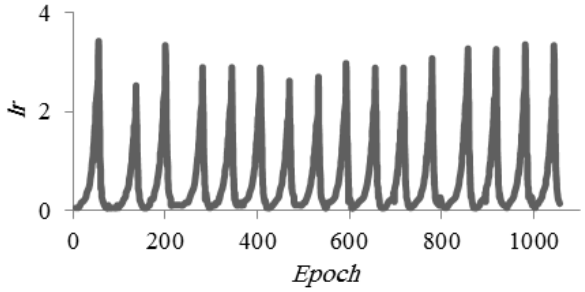

(c)

Fig.15
Networks training procesures to obtain desired precision. a) Gradient: 0.00124, b) Verification, c) Training Speed: 0.00308 at 1064 epoch.

4 RESULTS AND DISCUSSION

As considered in Fig.16 for specimens 2, 17 and 4 which are shown by red color, in 350(A) current the amount of crack propagating energy decreases as the feed rate increases. On the other hand, in specimens 12, 14 and 13 which are displaced by green color, in 400 (A) current the crack propagating energy increases by feed rate enhancement. This event could be justified by that in low electrical current, the lack of penetration occurs. Which the feed rate enhancement also intensifies this event and eventually the resistance of crack propagating decreases. On the other hand, the higher electrical current leads to complete penetration in addition feed rate reduction increases the heat flux applied to weld pool which finally leads to large microstructure and less crack propagating energy.

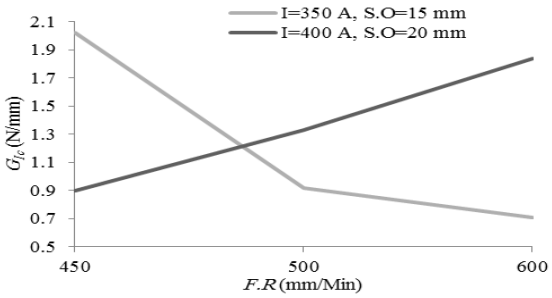

Fig.16
Influence of feed rate on crack propagating energy at constant electrical current.

Also the influence of electrical current was investigated in Fig.17. As observed for specimen 2, 18 and 8 which are shown by yellow color, at 450 ($\frac{mm}{\min}$) feed rate electrical current enhancement leads a fall in crack propagating resistance. On the other hand, for specimens 6, 11 and 16 at 500 ($\frac{mm}{\min}$) feed rate the increase in electrical current results in crack propagating energy enhancement. This trend also occurs for specimens 5, 1 and 17 namely the electrical current enhancement at 550 ($\frac{mm}{\min}$) feed rate eventuate in crack propagating energy increase. The aforementioned explanation in previous paragraph could be also true in this part so that in high feed rate, the lack of penetration occurs thus electrical current enhancement which leads to penetration increscent, raises the crack propagating resistance. On the other hand, low feed rate leads to complete penetration and so the applied heat flux to the weld pool controls the crack growth energy. Also because of increase in heat flux in high electrical currents, it could be deduced that high electrical currents lead to low crack propagating energy.

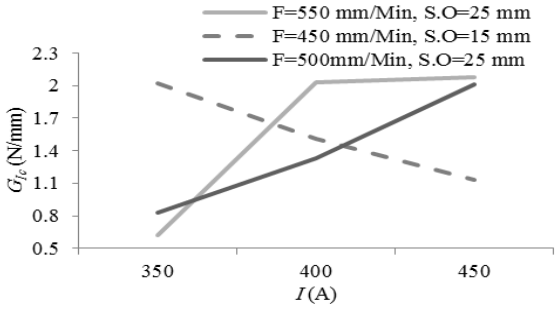

Fig.17
Influence of electrical current on crack propagating energy at constant feed rate.

After network training, using the experimental data, half of which coming from training data and the others half form new data. the precision of network performance was investigated. By importing input parameters, the modeled network estimates the value of crack propagating energy. Real value, estimated value, their comparison and the error rate of Output parameters are represented in Fig.18 and Table 7. It's observed that the network has 92.36% average precision.

Table 7
Crack growth energy estimation using the neural network.

Number	Real G_{lc} (*N/mm*)	Estimated G_{lc} (*N/mm*)	Accuracy Percent
5	1.85	1.53	84.4
8	1.13	0.99	87.6
13	1.84	1.56	83.2
19	1.70	1.63	95.9
20	1.11	1.02	91.9
21	1.72	1.63	94.8

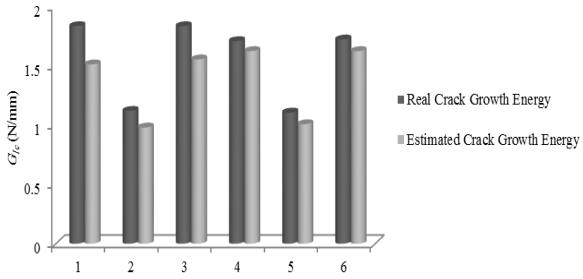

Fig.18
Networks estimation results compresion with real values.

6 CONCLUSIONS

Eventually, it can be induced that in high electrical current the presence of large microstructure is very feasible. It is due to the presence of high heat flux applied to weld pool and low cooling rate of process. It leads to a reduce in crack propagating resistance. Thus in high electrical current, feed rate enhancements could eradicate this phenomenon. On the other hand, in low electrical current, appearance of lack of penetration and lack of fusion are a dominant factor and determine attachment quality. So due to low heat flux the complete penetration doesn't occur and attachment resistance decreases. Also it is considered that using neural network; nonlinear properties could be predicted accurately. In this article the neural network designed to estimate crack propagating energy in welded attachments with less than 7.64% errors. It's recommended that influence of welding parameters on heat affected zone (HAZ) width and penetration depth be investigated. Also it would be beneficial that the effect of back propagating number on network accuracy be verified. It's offered that same specimens under same condition using various welding processes such as TIG, MIG and etc. be welded and the crack propagating energy of various processes be compared.

REFERENCES

[1] Yawar J., Lal H., 2015, Effect of various parameters on flux consumption, carbon and silicon in submerged arc welding (Saw),*International Journal on Emerging Technologies* **6**(2):176-180.

[2] Sharma M., Gupta D., Karun., 2014, Submerged arc welding: A review, *International Journal of Current Engineering and Technology* **4**(3): 1814-1817.

[3] Yang Y., 2008, *The Effect of Submerged Arc Welding Parameters on the Properties of Pressure Vessel and Wind Turbine Tower Steels*, University of Saskatchevan.

[4] Murugan N., Gunaraj V., 2005, Prediction and control of weld bead geometry and shape relationships in submerged arc welding of pipes, *Journal of Materials Processing Technology* **168**(3): 478-487.

[5] Dhas J.E.R., Kumanan S., 2010, Weld quality prediction of submerged arc welding process using a function replacing hybrid system, *Advances in Production Engineering & Management* **5**: 5-12.

[6] Juang S.C., Tarng Y.S., 2002, Process parameter selection for optimizing the weld pool geometry in the tungsten inert gas welding of stainless steel, *Journal of Materials Processing Technology* **122**(1): 33-37.

[7] Yang L.J., Bibby M.J., Chandel R.S., 1993, Linear regression equations for modeling the submerged-arc welding process, *Journal of Materials Processing Technology* **39**(1-2): 33-42.

[8] Murugan N., Gunaraj V., 2005, Prediction and control of weld bead geometry and shape relationships in submerged arc welding of pipes, *Journal of Materials Processing Technology* **168**(3): 478-487.

[9] Reed R.P., 1983, *The Economic Effects of Fracture in the United States*, US Department of Commerce, National Bureau of Standards.

[10] Hasson D.F., Zanis C.A., Anderson D.R., 1984, Fracture toughness of HY-130 steel weld metals, *Welding Journal* **63**(6):197-202.

[11] Om H., Pandey S., 2013, Effect of heat input on dilution and heat affected zone in submerged arc welding process, *Sadhana* **38**(6): 1369-1391.

[12] Shen S., Oguocha I.N.A., Yannacopoulos S., 2012, Effect of heat input on weld bead geometry of submerged arc welded ASTM A709 Grade 50 steel joints, *Journal of Materials Processing Technology* **212**(1): 286-294.

[13] Cretegny L., Saxena A., 1998, Fracture toughness behavior of weldments with mis-matched properties at elevated temperature, *International Journal of Fracture* **92**(2): 119-130.

[14] Zúñiga D.F., Kalthoff J.F., Canteli A.F., Grasa J., Doblaré M., 2013, Upper shelf fracture toughness of as welded manual metal arc weld metal, *ECF15*.
[15] Irwin G.R., 1948, Fracture dynamics, *Fracturing of Metals* **1948**: 147-166.